

# Driving the Berry phase anomalous Hall effect in a noncollinear antiferromagnet by domain manipulation

Yuchuan Yao,<sup>1, †</sup> Pratap Pal,<sup>1, †</sup> Neil G. Campbell,<sup>2</sup> Gautam Gurung,<sup>3</sup> Roger D. Johnson,<sup>4,5</sup> Pascal Manuel,<sup>6</sup> Evgeny Y. Tsymbal,<sup>3</sup> Mark S. Rzchowski<sup>2</sup> and Chang-Beom Eom<sup>1\*</sup>

<sup>1</sup>Department of Materials Science and Engineering, University of Wisconsin-Madison, Wisconsin 53706, USA.

<sup>2</sup>Department of Physics, University of Wisconsin-Madison, Wisconsin 53706, USA.

<sup>3</sup>Department of Physics and Astronomy & Nebraska Center for Materials and Nanoscience, University of Nebraska, Lincoln, NE 68588, USA

<sup>4</sup>Department of Physics and Astronomy, University College London, London, WC1E 6BT, United Kingdom.

<sup>5</sup>London Centre for Nanotechnology, University College London, London WC1E 6BT, United Kingdom.

<sup>6</sup>ISIS Facility, STFC Rutherford Appleton Laboratory, Didcot, Oxfordshire OX11 0QX, United Kingdom.

\*Corresponding author: [ceom@wisc.edu](mailto:ceom@wisc.edu)

†These authors contributed equally.

## Abstract

The emergence of anomalous Hall effects (AHE) in antiferromagnets presents an intriguing phenomenon with potential spintronic device applications due to their ultrafast switching dynamics.  $\text{Mn}_3\text{NiN}$  antiperovskite stands out as a promising candidate owing to its noncollinear antiferromagnetism. In this study, we report a significant AHE observed in epitaxial  $\text{Mn}_3\text{NiN}$  thin films below the Néel temperature, comparable to those observed in typical ferromagnets. Through a combination of magnetometry, neutron diffraction and *ab-initio* data analyses, we propose that the substantial AHE can be attributed to the non-vanishing Berry curvature arising from the  $\Gamma^{4g}$ -type spin structure, coupled with uncompensated magnetic domains featuring a weak canted moment. This coupling, due to robust antiferromagnetic domains, enables deterministic detection and switching of AHE via the application of a magnetic field.

## Introduction

Understanding and manipulating the coupling of electronic spin and charge in antiferromagnets offers a plethora of promising applications with the advantages of lack of stray fields, low susceptibility to external perturbations, and ultrafast spin dynamics [1–10]. However, the absence of net magnetization presents significant challenges for the detection and control of the antiferromagnetic (AFM) state [3]. Recent progress has come from the discovery of a large anomalous Hall effect (AHE) in noncollinear antiferromagnets (NCAFs) such as Mn based hexagonal  $\text{Mn}_3\text{Sn}$  [11] or  $\text{Mn}_3\text{Ge}$  [12], cubic  $\text{Mn}_3\text{Pt}$  [13] or  $\text{Mn}_3\text{Ir}$  [14] and antiperovskites  $\text{Mn}_3\text{XN}$  ( $X=\text{Ga}$  [15],  $\text{Sn}$  [16] and  $\text{Ni}$  [17]). These NCAFs have magnetic moments in the (111) Kagome plane nearly or fully compensated [10,11], thus precluding a simple origin of the AHE in these systems driven by the net magnetic moment. However, recent theoretical studies have highlighted the role of spin-orbit-coupling with the simultaneous absence of symmetries (e.g. mirror symmetries in  $\Gamma^{4g}$  phase of  $\text{Mn}_3\text{NiN}$ ), in making the sum of Berry curvature over the Brillouin zone non-zero [18,19], resulting in a nonzero AHE.

Berry curvature induced AHE in such NCAFs is an intriguing phenomenon with wide-ranging applications. For example, the AHE in bulk  $\text{Mn}_3\text{Sn}$  changes sign under strain from positive to negative [20]. Similarly, the AHE in  $\text{Mn}_3\text{Pt}$  thin film is vanishingly small in its cubic phase at higher thickness, but emerges as soon as tetragonal phase is stabilized at reduced thickness [21,22]. A holistic understanding of the origin and controllability (by external parameters such as magnetic field) of AHE in such NCAFs is important. Along with this, high-quality epitaxial thin films are needed towards potential device applications. In this regard,  $\text{Mn}_3\text{Sn}$  and  $\text{Mn}_3\text{Ge}$  have been extensively studied [11,12]. Antiperovskite  $\text{Mn}_3\text{XN}$  materials have been predicted to exhibit even larger AHE compared to their  $\text{Mn}_3\text{X}$  counterparts [23]. But the structural dissimilarity of the antiperovskite structure (Fig. 1(a)) with commercially available oxide perovskite substrates has presented challenges to epitaxial growth of high-quality films [15]. Here we report significant advances in noncollinear AFM  $\text{Mn}_3\text{NiN}$  epitaxial thin films with antiperovskite structure, which recently showed an AHE [17] that has been argued to originate directly from the Berry curvature in the electronic band structure [14,18].

In this letter, we demonstrate the growth of high-quality atomically smooth epitaxial  $\text{Mn}_3\text{NiN}$  thin films, determination of their AFM properties, and the observation of a large AHE correlated with the AFM domain structure. Our films show noncollinear  $\Gamma^{4g}$  magnetic ordering (illustrated in Fig. 1(a)) below the Néel temperature ( $T_N$ ) of 240 K that retains this symmetry to 2 K. Importantly, we observe a large AHE around  $T_N$  comparable in size to common *ferromagnets*, even though the films show a net moment of only  $8 \text{ m}\mu_B/\text{Mn}$  (arising from a small distortion of the non-collinear  $\Gamma^{4g}$ -spin arrangement in the (111) plane). This large AHE in the absence of a significant net moment suggests a Berry phase mechanism, and the weak moment provides a controllability to switch AFM domains, and hence the AHE, with applied magnetic field, as illustrated in Figs. 1(b) and (c). The AFM domain texture gives rise to the non-zero Berry curvature and therefore, the observed large AHE, as corroborated from our *first-principle* calculations. Such a controllability of AFM domain assisted AHE in  $\text{Mn}_3\text{NiN}$  can pave a path for exploration of non-volatile AFM-spintronic device applications in many other similar systems.

Epitaxial 40 nm  $\text{Mn}_3\text{NiN}$  thin films were grown on (001)-oriented  $(\text{La}_{0.3}\text{Sr}_{0.7})(\text{Al}_{0.65}\text{Ta}_{0.35})\text{O}_3$  (LSAT) substrates by DC reactive magnetron sputtering. Further characterization details can be found in section I of Supplemental Material [24].

Antiperovskite nitride thin-film growth on oxide perovskite substrates offers significant challenges, as the films are metallic and have perovskite crystal structure (with a space group  $Pm\bar{3}m$ ) with cation and anion positions interchanged in the unit cell in comparison to perovskite  $\text{ABO}_3$  substrate, as shown in Figs. S2(a) and (b) of the Supplemental Material [24]. Whereas  $\text{ABO}_3$  perovskites can be viewed as alternate stackings of  $\text{AO}$  and  $\text{BO}_2$  layers along the [001] direction,  $\text{Mn}_3\text{XN}$  can be described as similar stackings of  $\text{MnX}$  and  $\text{Mn}_2\text{N}$  layers as illustrated in Fig. S2(c) of the Supplemental Material [24]. Importantly, we were able to grow high quality  $\text{Mn}_3\text{NiN}$  thin-films on LSAT substrates through optimized growth condition, as clearly visible from the out-of-plane XRD of (002) peak, shown in Fig. 2(a) (also note Fig. S3 of the Supplemental Material [24]). A strong  $\text{Mn}_3\text{NiN}$  peak is observed along with distinct Kiessig fringes, indicating high crystalline quality and a pristine interface with the substrate. This is further corroborated by the streaky RHEED pattern after growth and X-ray reflectivity data as shown in the inset to Fig. 2(a) and Fig. S4(a) of the Supplemental Material [24]. The narrow  $0.029^\circ$  full width at half maximum (FWHM) of the rocking curve for  $\text{Mn}_3\text{NiN}$  (002) (shown in Fig. S4(b) of the Supplemental Material [24]) further supports high crystalline quality. The phi scans on the asymmetric  $(\bar{1}13)$  peak of  $\text{Mn}_3\text{NiN}$  and LSAT, shown in Fig. S5(a) of the Supplemental Material [24], indicate the in-plane cube-on-cube epitaxial relationship. X-ray reciprocal space mapping (RSM) measurements centered on the asymmetrical  $(\bar{1}13)$  peak, shown in Fig. S5(b) of the Supplemental Material [24], indicate that  $c/a=0.9952$  at room-temperature. Atomic force microscope imaging shows an atomically smooth surface with a roughness of  $\sim 0.3$  nm (Fig. 2(b)). All these data strongly indicate high-quality epitaxial growth of  $\text{Mn}_3\text{NiN}$  thin films, for which magnetic and transport measurements can probe fundamental properties.

Figure 2(c) shows temperature dependence of the out-of-plane magnetic moment. From the variation of magnetization with temperature, we clearly note a deviation between field-cooling (FC) and zero-field-cooling (ZFC) curves below the Néel temperature of 240 K (note Fig. S6(a) of the Supplemental Material for the in-plane magnetization data [24]). A field-cooled magnetic moment of  $\sim 0.008 \mu_{\text{B}}/\text{Mn}$  indicates the presence of a weak ferromagnetic moment, similar to that observed in other non-collinear AFM materials [10,11]. While a net moment is unexpected in a perfectly compensated antiferromagnet (e.g., in bulk cubic  $\text{Mn}_3\text{NiN}$ ), thin films with tetragonal distortions ( $c \neq a$ ) and accompanying strain are expected to have a weak moment in both in-plane and out-of-plane directions [10,25,26], sometimes referred to as piezomagnetism [25]. This reflects a weak net moment that lies in the (111) plane inclined relative to the substrate, as illustrated in Fig. 1(c). Isothermal magnetic field sweeps above and below the Neel temperature (Fig. 2(d)) show hysteretic behavior at 230K (below  $T_{\text{N}}$ ) with a weak saturation moment consistent with the field-cooled measurement of Fig. 2(c), and nonhysteretic behavior at 240K (above  $T_{\text{N}}$ ). At 230K the applied out-of-plane magnetic field switches the weak net moment with a coercive field of a 0.4 T and a saturation field of several Tesla. The relatively large coercive field suggests strong crystalline anisotropy [27]. The  $\sim 0.008 \mu_{\text{B}}/\text{Mn}$  saturation moment is much smaller than the  $2.7 \mu_{\text{B}}/\text{Mn}$  moment that would arise from fully-aligned Mn spins in this structure [29,30]. This further supports the scenario that the distortion has only slightly perturbed the AFM alignment of

Mn<sub>3</sub>NiN spins. This weak ferromagnetic moment in Mn<sub>3</sub>NiN allows a control of its AFM state and related emergent properties.

The impact of magnetism on film resistivity was characterized in a four-corner van der Pauw geometry where longitudinal and transverse resistivities were determined. The longitudinal resistivity corroborates the  $M$ - $T$  data by showing a clear kink at 240 K, as shown in Fig. 3(a). Above  $T_N$  the resistivity is nearly flat with temperature and becomes strongly metallic below  $T_N$  with Residual Resistivity Ratio (RRR) of  $\sim 2.5$  (Fig. S6(b)). The transverse resistivity in the Hall geometry shows a transition from a linear dependence on magnetic field above  $T_N$  consistent with an ordinary Hall effect, to a highly nonlinear field dependence with a clear hysteresis below  $T_N$ , as shown in Fig. 3(b), indicating contribution from a nontrivial AHE. We found identical results in a patterned Hall-bar device ( Fig. S7 of the Supplemental Material [24] ). We extracted the AHE component by subtracting the high-field linear part from the total Hall signal. Figure S7(b) of the Supplemental Material [24] shows that the resulting AHE component has a hysteretic behavior at low applied magnetic field, and saturation at high magnetic field. The high-field saturation value, which we will argue arises from AFM domain alignment, we define as  $\rho_{\text{AHE}}$ .

Figure 3(c) shows the temperature dependence of  $\rho_{\text{AHE}}$ , indicating a maximum value of about  $1 \mu\Omega\text{-cm}$ . This large value is comparable to common ferromagnetic metals such as  $0.6 \mu\Omega\text{-cm}$  for Fe with net moment  $2.18 \mu_B/\text{Fe}$ ,  $0.1 \mu\Omega\text{-cm}$  for Co with moment  $1.67 \mu_B/\text{Co}$ , and  $0.15 \mu\Omega\text{-cm}$  for Ni with moment  $0.62 \mu_B/\text{Ni}$  [30–34], all of which have dramatically larger ferromagnetic moments than the  $0.008 \mu_B/\text{Mn}$  in our Mn<sub>3</sub>NiN films, which is too small to generate a signal of  $\rho_{\text{AHE}}$  of  $\sim 1 \mu\Omega\text{-cm}$  [11]. This large  $\rho_{\text{AHE}}$  of Mn<sub>3</sub>NiN films is also comparable to other non-collinear antiferromagnets as shown in Fig. S8 of the Supplemental Material [24]. This is consistent with a non-vanishing Berry curvature from the  $\Gamma^{4g}$  spin structure, capable of inducing such a large AHE [14,28,35]. We conclude that the effect of the net moment is secondary in generating the observed AHE. Comparing the anomalous behavior of  $\rho_{\text{AHE}}$  with the net moment, as shown in Fig. S9 of the Supplemental Material [24], further supports this conclusion.

The temperature dependent behavior of  $\rho_{\text{AHE}}$  (Fig. 3(c)) indicates that above  $T_N$   $\rho_{\text{AHE}}$  is temperature independent and very small, while immediately below  $T_N$   $\rho_{\text{AHE}}$  increases to large values ( $\sim 1 \mu\Omega\text{-cm}$ ) before gradually dropping to zero as temperature is decreased. We divide this behavior into temperature regions: region I, where the AHE is large and region II where it is almost zero. A similar temperature dependence has been reported for a related system: Mn<sub>3</sub>Pt thin films, where the anomalous behavior in  $\rho_{\text{AHE}}$  was correlated with a reduction of half-order magnetic diffraction peak intensities of bulk Mn<sub>3</sub>Pt [13] that indicated a change in magnetic order. We investigated this possibility with temperature dependent neutron diffraction measurements on Mn<sub>3</sub>NiN thin films as shown in Fig. 3(d) [24]. The Mn<sub>3</sub>NiN (001) magnetic diffraction peak was observed below  $T_N$ , consistent with the onset of long-range AFM  $\Gamma^{4g}$  spin ordering. The magnetic peak intensity remains almost constant down to 2 K, unlike in Mn<sub>3</sub>Pt [31], indicating that no magnetic transitions from the  $\Gamma^{4g}$  phase occur in these Mn<sub>3</sub>NiN films. Hence the temperature dependence of  $\rho_{\text{AHE}}$  does not arise from any magnetic structure transition.

Here we argue that the distinct temperature dependence of the anomalous Hall resistivity arises from the behavior of AFM domains and their coupling to external magnetic fields through the weak ferromagnetic moment. Fig. 1(c) shows the eight different possible AFM domains in

Mn<sub>3</sub>NiN. They represent four domains lying in the four (111) planes (D1, D2, D3, D4) and each having time-reversal pairs (D1', D2', D3', D4'). Strain can induce a net moment, whose sign depends on whether all Mn spins point inwards or outwards in the (111) triangular plane. As the spin configuration couples directly to the Berry curvature, an equal population of all domains will lead to a zero AHE. However, the domain population can become biased by small external fields near T<sub>N</sub>, giving rise to a nonzero AHE. To investigate this possibility, we made Hall measurements at 210K (region I) and 20 K (region II) after cooling the sample at positive, zero and negative applied fields as shown in Figs. 4(a) and (b). The spontaneous (zero-field) anomalous Hall resistivity in region I near T<sub>N</sub> is almost zero for zero-field-cooling, and positive (negative) for +2 T (-2 T) field cooling. At larger applied field after the different field cooling, the different anomalous Hall resistivity depends on applied field. This indicates that the applied field controls the AFM domain configuration. At 20 K (region II), the zero-field behavior is similar, but the absence of magnetic field dependence indicates complete freezing of AFM domains at low temperature as shown in Fig. 4(b) (also note Fig. S9), likely due to increased magnetic anisotropy.

We further explored this by cooling the sample under applied magnetic field ranging from 0 to -10T at 210K and making Hall measurements as shown in Fig. S11 of the Supplemental Material [24]. The inset to Fig. 4(a) shows the variation of anomalous Hall resistivity (the value at  $H = 0$ ) with applied cooling field, indicating that  $\rho_{\text{AHE}}$  saturates beyond 3 T, suggesting the alignment of all magnetic domains. At the temperature just below T<sub>N</sub> (region I), a significant fraction of AFM domains are switched by changing the external magnetic field. This orientation of AFM domains contribute to the large value of AHE in the Mn<sub>3</sub>NiN films. At much lower temperature (region II), the increased magnetic anisotropy prevents even an applied field of 10 T from switching AFM domains, resulting in net zero AHE.

To confirm this conclusion, we performed first-principle calculations of the anomalous Hall conductivity of Mn<sub>3</sub>NiN with the  $\Gamma^{4g}$  spin ordering [18,19]. Figure 4(c) shows the calculated Berry curvature within the  $(\bar{1}10)$  plane of the Brillouin zone for a single AFM domain. While the Berry curvature is nearly zero over the large portion of this plane, it is sizable at the points where the Fermi surface sheets touch each other (at the  $\Gamma$ -Z line) and near the R points, thus contributing to the large AHE. By symmetry, the anomalous Hall conductivity  $\sigma_{xy}$  is equal in magnitude for all eight domains shown in Fig 1(c). Domains D1 and D2 have the same sign of  $\sigma_{xy}$  which is opposite to the sign to  $\sigma_{xy}$  in domains D3 and D4. By time reversal symmetry, domains D1'-D4' have  $\sigma_{xy}$  opposite to that in domains D1-D4. This leads to a nominal zero  $\sigma_{xy}$  for equal populations of all AFM domains (Fig. 4(d)), consistent with our positive, negative and ZFC anomalous Hall data shown in Fig. 4(a). When the AFM domain populations are not equal, as occurs in our experiments when the sample is cooled in an external magnetic field, the contributions to  $\sigma_{xy}$  from different domains become uncompensated the net anomalous Hall conductivity turns to non-zero.

## Conclusion

We have demonstrated growth of high-quality epitaxial antiperovskite Mn<sub>3</sub>NiN thin films on perovskite LSAT substrates, which exhibit a paramagnetic to noncollinear  $\Gamma^{4g}$ -type AFM transition near 240 K. These Mn<sub>3</sub>NiN thin films exhibit a concomitant large anomalous Hall effect in the AFM state whose magnitude is comparable to typical ferromagnets, although these

noncollinear AFM have almost zero net moment. The origin of such a large AHE lies in the non-vanishing Berry curvature, specific to each AFM domain. The AHE is switchable and controllable by external magnetic field due to a coupling of AFM domains to a weak domain-dependent net magnetic moment. This demonstration and understanding of the AFM domain control of AHE in the simple noncollinear AFM  $\text{Mn}_3\text{NiN}$  provides a path toward new AHE-based spintronic systems.

### **Acknowledgement**

CBE acknowledges support for this research through a Vannevar Bush Faculty Fellowship (ONR N00014-20-1-2844), and the Gordon and Betty Moore Foundation's EPIQS Initiative, Grant GBMF9065. Transport measurement at the University of Wisconsin–Madison was supported by the US Department of Energy (DOE), Office of Science, Office of Basic Energy Sciences (BES), under award number DE-FG02-06ER46327.

## References

- [1] S. D. Bader and S. S. P. Parkin, *Spintronics*, *Annu. Rev. Condens. Matter Phys.* **1**, 71 (2010).
- [2] I. Žutić, J. Fabian, and S. Das Sarma, *Spintronics: Fundamentals and Applications*, *Rev. Mod. Phys.* **76**, 323 (2004).
- [3] V. Baltz, A. Manchon, M. Tsoi, T. Moriyama, T. Ono, and Y. Tserkovnyak, *Antiferromagnetic Spintronics*, *Rev. Mod. Phys.* **90**, 015005 (2018).
- [4] R. O. Cherifi, V. Ivanovskaya, L. C. Phillips, A. Zobelli, I. C. Infante, E. Jacquet, V. Garcia1, S. Fusil1, P. R. Briddon, N. Guiblin, A. Mougin, A. A. Ūnal, F. Kronast, S. Valencia, B. Dkhil, A. Barthélemy, and M. Bibes, *Electric-Field Control of Magnetic Order above Room Temperature*, *Nat. Mater.* **13**, 345 (2014).
- [5] A. Bose, N. J. Schreiber, R. Jain, D. F. Shao, H. P. Nair, J. Sun, X. S. Zhang, D. A. Muller, E. Y. Tsymbal, D. G. Schlom, and D. C. Ralph, *Tilted Spin Current Generated by the Collinear Antiferromagnet Ruthenium Dioxide*, *Nat. Electron.* **5**, 267 (2022).
- [6] P. Wadley, B. Howells, J. Železný, C. Andrews, V. Hills, R. P. Campion, V. Novák, K. Olejník, F. Maccherozzi, S. S. Dhesi, S. Y. Martin, T. Wagner, J. Wunderlich, F. Freimuth, Y. Mokrousov, J. Kuneš, J. S. Chauhan, M. J. Grzybowski, A. W. Rushforth, Kw. Edmond, B. L. Gallagher, and T. Jungwirth, *Electrical Switching of an Antiferromagnet*, *Science* **351**, 587 (2016).
- [7] X. Chen, T. Higo, K. Tanaka, T. Nomoto, H. Tsai, H. Idzuchi, M. Shiga, S. Sakamoto, R. Ando, H. Kosaki, T. Matsuo, D. Nishio-Hamane, R. Arita, S. Miwa, and S. Nakatsuji, *Octupole-Driven Magnetoresistance in an Antiferromagnetic Tunnel Junction*, *Nature* **613**, 490 (2023).
- [8] P. Qin, H. Yan, X. Wang, H. Chen, Z. Meng, J. Dong, M. Zhu, J. Cai, Z. Feng, X. Zhou, L. Liu, T. Zhang, Z. Zeng, J. Zhang, C. Jiang and Z. Liu , *Room-Temperature Magnetoresistance in an All-Antiferromagnetic Tunnel Junction*, *Nature* **613**, 485 (2023).
- [9] T. Nan, C. X. Quintela, J. Irwin, G. Gurung, D. F. Shao, J. Gibbons, N. Campbell, K. Song, S. -Y. Choi, L. Guo, R. D. Johnson, P. Manuel, R. V. Chopdekar, I. Hallsteinsen, T. Tybell, P. J. Ryan, J. -W. Kim, Y. Choi, P. G. Radaelli, D. C. Ralph, E. Y. Tsymbal, M. S. Rzchowski and C. B. Eom , *Controlling Spin Current Polarization through Non-Collinear Antiferromagnetism*, *Nat. Commun.* **11**, 4671 (2020).
- [10] D. Boldrin, A. P. Mihai, B. Zou, J. Zemen, R. Thompson, E. Ware, B. V. Neamtu, L. Ghivelder, B. Esser, D. W. McComb, P. Petrov, and L. F. Cohen , *Giant Piezomagnetism in Mn<sub>3</sub>NiN*, *ACS Appl. Mater. Interfaces* **10**, 18863 (2018).
- [11] S. Nakatsuji, N. Kiyohara, and T. Higo, *Large Anomalous Hall Effect in a Non-Collinear Antiferromagnet at Room Temperature*, *Nature* **527**, 212 (2015).
- [12] N. Kiyohara, T. Tomita, and S. Nakatsuji, *Giant Anomalous Hall Effect in the Chiral Antiferromagnet Mn<sub>3</sub>Ge*, *Phys. Rev. Appl.* **5**, 064009 (2016).
- [13] S. Novakov, P. B. Meisenheimer, G. A. Pan, P. Kezer, N. M. Vu, A. J. Grutter, R. F. Need, J. A. Mundy, and J. T. Heron, *Composite Spin Hall Conductivity from Non-Collinear Antiferromagnetic Order*, *Adv. Mater.* **35**, 2209866 (2023).
- [14] H. Chen, Q. Niu, and A. H. Macdonald, *Anomalous Hall Effect Arising from Noncollinear Antiferromagnetism*, *Phys. Rev. Lett.* **112**, 017205 (2014).
- [15] C. X. Quintela, K. Song, D. F. Shao, L. Xie, T. Nan, T. R. Paudel, N. Campbell, X. Pan, T. Tybell, M. S. Rzchowski, E. Y. Tsymbal, S. Y. Choi [https](https://doi.org/10.1126/sciadv.aba4017), and C. B. Eom , *Epitaxial Antiperovskite/Perovskite Heterostructures for Materials Design*, *Sci. Adv.* **6**, eaba4017 (2020).

- [16] B. H. Rimmler, B. K. Hazra, B. Pal, K. Mohseni, J. M. Taylor, A. B. Pinto, H. Deniz, M. Tangi, I. Kostanovskiy, C. Luo, R. R. Neumann, A. Ernst, F. Radu, I. Mertig, H. L. Meyerheim, S. S. P. Parkin, *Atomic Displacements Enabling the Observation of the Anomalous Hall Effect in a Non-Collinear Antiferromagnet*, *Adv. Mater.* **35**, 2209616 (2023).
- [17] D. Boldrin, I. Samathrakris, J. Zemen, A. Mihai, B. Zou, F. Johnson, B. D. Esser, D. W. McComb, P. K. Petrov, H. Zhang, and L. F. Cohen, *Anomalous Hall Effect in Noncollinear Antiferromagnetic Mn<sub>3</sub>NiN Thin Films*, *Phys. Rev. Mater.* **3**, 094409 (2019).
- [18] G. Gurung, D. F. Shao, T. R. Paudel, and E. Y. Tsymbal, *Anomalous Hall Conductivity of Noncollinear Magnetic Antiperovskites*, *Phys. Rev. Mater.* **3**, 044409 (2019).
- [19] G. Gurung, D. F. Shao, and E. Y. Tsymbal, *Spin-Torque Switching of Noncollinear Antiferromagnetic Antiperovskites*, *Phys. Rev. B* **101**, 140405(R) (2020).
- [20] M. Ikhlas, S. Dasgupta, F. Theuss, T. Higo, S. Kittaka, B. J. Ramshaw, O. Tchernyshyov, C. W. Hicks, and S. Nakatsuji, *Piezomagnetic Switching of the Anomalous Hall Effect in an Antiferromagnet at Room Temperature*, *Nat. Phys.* **18**, 1086 (2022).
- [21] Z. Q. Liu et al., *Electrical Switching of the Topological Anomalous Hall Effect in a Non-Collinear Antiferromagnet above Room Temperature*, *Nat. Electron.* **1**, 172 (2018).
- [22] B. E. Zuniga-Cespedes, K. Manna, H. M. L. Noad, P. Y. Yang, M. Nicklas, C. Felser, A. P. Mackenzie, and C. W. Hicks, *Observation of an Anomalous Hall Effect in Single-Crystal Mn<sub>3</sub>Pt*, *New J. Phys.* **25**, 023029 (2023).
- [23] V. T. N. Huyen, M. T. Suzuki, K. Yamauchi, and T. Oguchi, *Topology Analysis for Anomalous Hall Effect in the Noncollinear Antiferromagnetic States of Mn<sub>3</sub>A N (A=Ni, Cu, Zn, Ga, Ge, Pd, In, Sn, Ir, Pt)*, *Phys. Rev. B* **100**, 094426 (2019).
- [24] *Supplemental Material*, (URL will be provided by the publisher).
- [25] P. Lukashev, R. F. Sabirianov, and K. Belashchenko, *Theory of the Piezomagnetic Effect in Mn-Based Antiperovskites*, *Phys. Rev. B*, **78**, 184414 (2008).
- [26] J. Zemen, Z. Gercsi, and K. G. Sandeman, *Piezomagnetism as a Counterpart of the Magnetovolume Effect in Magnetically Frustrated Mn-Based Antiperovskite Nitrides*, *Phys. Rev. B* **96**, 024451 (2017).
- [27] B. Dieny and M. Chshiev, *Perpendicular Magnetic Anisotropy at Transition Metal/Oxide Interfaces and Applications*, *Rev. Mod. Phys.* **89**, 025008 (2017).
- [28] K. Zhao, T. Hajiri, H. Chen, R. Miki, H. Asano, and P. Gegenwart, *Anomalous Hall Effect in the Noncollinear Antiferromagnetic Antiperovskite Mn<sub>3</sub>Ni<sub>1-x</sub>Cu<sub>x</sub>N*, *Phys. Rev. B* **100**, 045109 (2019).
- [29] J. F. Ding, O. I. Lebedev, S. Turner, Y. F. Tian, W. J. Hu, J. W. Seo, C. Panagopoulos, W. Prellier, G. Van Tendeloo, and T. Wu, *Interfacial Spin Glass State and Exchange Bias in Manganite Bilayers with Competing Magnetic Orders*, *Phys. Rev. B* **87**, 054428 (2013).
- [30] Y. Yang, Z. Luo, H. Wu, Y. Xu, R. W. Li, S. J. Pennycook, S. Zhang, and Y. Wu, *Anomalous Hall Magnetoresistance in a Ferromagnet*, *Nat. Commun.* **9**, 2255 (2018).
- [31] Y. Tian, L. Ye, and X. Jin, *Proper Scaling of the Anomalous Hall Effect*, *Phys. Rev. Lett.* **103**, 087206 (2009).
- [32] D. Hou, Y. Li, D. Wei, D. Tian, L. Wu, and X. Jin, *The Anomalous Hall Effect in Epitaxial Face-Centered-Cubic Cobalt Films*, *J. Phys. Condens. Matter* **24**, 482001 (2012).
- [33] I. M. L. Billas, A. Châtelain, and W. A. de Heer, *Magnetism from the Atom to the Bulk in Iron, Cobalt, and Nickel Clusters*, *Science* **265**, 1682 (1994).



- [34] L. Ye, Y. Tian, X. Jin, and D. Xiao, *Temperature Dependence of the Intrinsic Anomalous Hall Effect in Nickel*, Phys. Rev. B **85**, 220403(R) (2012).
- [35] D. Boldrin, F. Johnson, R. Thompson, A. P. Mihai, B. Zou, J. Zemen, J. Griffiths, P. Gubeljak, K. L. Ormandy, P. Manuel, D. D. Khalyavin, B. Ouladdiaf, N. Qureshi, P. Petrov, W. Branford, L. F. Cohen *The Biaxial Strain Dependence of Magnetic Order in Spin Frustrated Mn<sub>3</sub>NiN Thin Films*, Adv. Funct. Mater. **29**, 1902502 (2019).

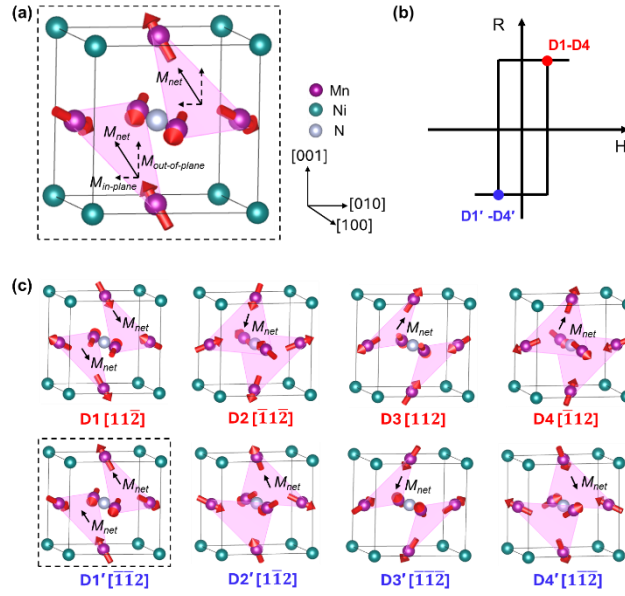


Fig 1: Schematic illustration of (a) antiperovskite  $\text{Mn}_3\text{NiN}$  with net moment induced from a distortion in  $\Gamma^{4g}$  spin structure, (b) domain contribution on berry curvature driven anomalous Hall effect in  $\text{Mn}_3\text{NiN}$ , and (c) all possible antiferromagnetic domain configurations of  $\text{Mn}_3\text{NiN}$  with their moment directions.

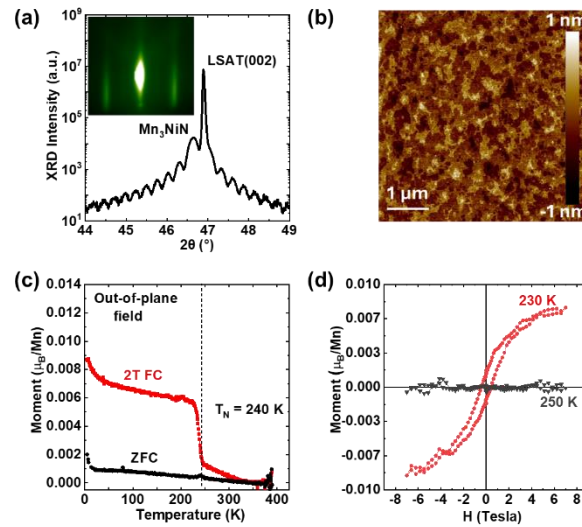


Fig 2: (a) Room-temperature out-of-plane XRD spectrum of  $\text{Mn}_3\text{NiN}$  thin-film around the (002) reflection of the LSAT substrate. Inset to (a) shows RHEED pattern of the specular diffraction spot after growth. (b) Atomically smooth atomic force microscopic morphology of  $\text{Mn}_3\text{NiN}$  thin-film. (c) Out-of-plane net magnetization vs temperature curves for 2 T field cooled (red) and zero-field-cooled (black), while measuring during warming in 0.5 T. Distinct Néel transitions are visible

around 240 K. (d) Net magnetization vs out-of-plane magnetic field showing clear weak net moment below  $T_N$ .

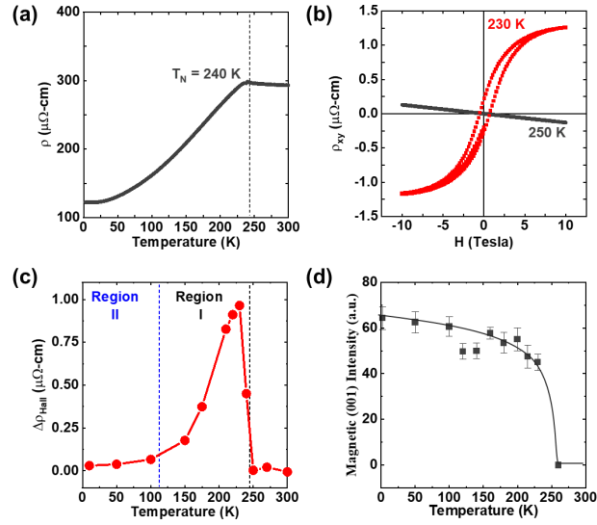


Fig 3: (a) Longitudinal resistivity  $\rho$  vs temperature curve indicating distinct slope change around  $T_N$ . (b) Hall resistivity vs out-of-plane magnetic field showing clear anomalous Hall signal below  $T_N$ . (c) Temperature dependence of anomalous Hall resistivity change ( $\rho_{AHE}$ ), shows maximum around the paramagnetic to  $\Gamma^{4g}$  transition and then, gradually decreases and becomes almost zero below  $\sim 100$  K. (d) Temperature dependence of neutron diffraction (001) peak intensity, showing an abrupt increase at the Neel temperature, and mostly temperature independence below  $T_N$ . The temperature independence indicates the absence of additional spin structure transitions below  $T_N$ .

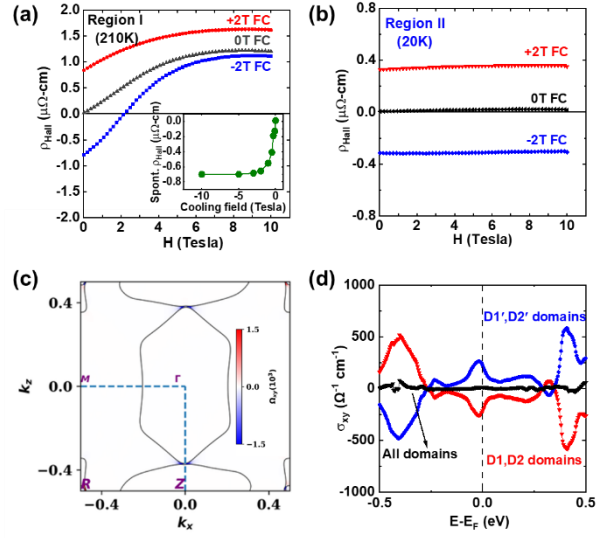


Fig 4: (a) Variation of the anomalous Hall resistivity with magnetic field while ramping the field from 0 T to 10 T at 210K, after cooling the sample under ZFC and +/- 2T FC. Inset to (a) shows variation of spontaneous Hall resistivity at different cooling field. (b) Variation of the anomalous Hall resistivity with magnetic field while ramping the field from 0 T to 10 T at 200K, after cooling the sample under ZFC and +/- 2T FC. (c) Heatmap of Berry curvature of one antiferromagnetic domain D1 of Mn<sub>3</sub>NiN at fermi surface in  $(\bar{1}10)$  plane. (d) Comparison of anomalous Hall effect of Mn<sub>3</sub>NiN with different antiferromagnetic domains.